Obrabotka metallov (tekhnologiya, oborudovanie, instrumenty) = Metal Working and Material Science. 2025 vol. 27 no. 1 pp. 48–60
ISSN: 1994-6309 (print) / 2541-819X (online)
DOI: 10.17212/1994-6309-2025-27.1-48-60

NSTU NETI

Obrabotka metallov - Metal Working and Material Science

Journal homepage: http://journals.nstu.ru/obrabotka_metallov

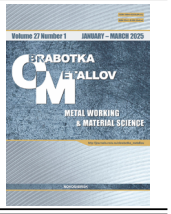

Prediction of changes in the surface layer during copy-piercing electrical discharge machining

Timur Ablyaz [a], ***Ilya Osinnikov*** [b], ***Evgeniy Shlykov*** [c, *], ***Anna Kamenskikh*** [d], ***Aleksandr Gorohov*** [e], ***Nikita Kropanev*** [f], ***Karim Muratov*** [g]

Perm National Research Polytechnic University, 29 Komsomolsky prospekt, Perm, 614990, Russian Federation

[a] https://orcid.org/0000-0001-6607-4692, lowrider11-13-11@mail.ru; [b] https://orcid.org/0009-0006-4478-3803, ilyuhaosinnikov@bk.ru;
[c] https://orcid.org/0000-0001-8076-0509, Kruspert@mail.ru; [d] https://orcid.org/0000-0002-3012-2418, anna_kamenskih@mail.ru;
[e] https://orcid.org/0009-0000-5588-0154, littlealex99@mail.ru; [f] https://orcid.org/0009-0002-5907-9852, cropanew.nikita2016@yandex.ru;
[g] https://orcid.org/0000-0001-7612-8025, Karimur_80@mail.ru

ARTICLE INFO

Article history:
Received: 13 December 2024
Revised: 19 December 2024
Accepted: 28 December 2024
Available online: 15 March 2025

Keywords:
Copy-piercing electrical discharge machining
Mathematical model
Chromium steel
Crater formation
Metallography
White layer
Continuity

Funding
The study was supported by the Russian Science Foundation grant No. 23-79-01224, https://rscf.ru/project/23-79-01224/.

ABSTRACT

Introduction. This paper presents the results of theoretical and experimental studies of the thickness, continuity and number of defects in the white layer formed during the copy-piercing electrical discharge machining, using low-alloy steel *0.4 C-Cr* and medium-alloy steel *0.35 C-Cr-Mn-Si* as an example. **The purpose of the work** is to theoretically and experimentally investigate the defective surface layer formed during copy-piercing electrical discharge machining. **Research methods.** Mathematical models of a single discharge pulse impact on the surface being machined were obtained using the finite element method. An *Electronica Smart CNC* copy-piercing electrical discharge machine was selected as the equipment for copy-piercing electrical discharge machining of samples made from *0.4 C-Cr* and *0.35 C-Cr-Mn-Si* steels. Simulating and experiments were carried out in two modes. The operating parameters were: pulse-on time (T_{on}, μs), voltage (U, V), and current (I, A). Metallographic studies were performed using an *OLYMPUS GX 51* optical microscope. **Results and discussion.** Mathematical models were developed to simulate the impact of a single discharge pulse on the machined surface during copy-piercing electrical discharge machining. These models allow predicting the thickness of the white layer depending on the processing modes and the properties of the material being processed. The theoretical values of the white layer thickness vary in the range of 20–25 μm during copy-piercing electrical discharge machining in the minimum mode and vary in the range of 60–80 μm in the maximum mode. It was established that the experimental values of the white layer thickness vary in the range of 20–25 μm during copy-piercing electrical discharge machining in the minimum mode and vary in the range of 55–85 μm in the maximum mode. The deviation of the theoretical values of the white layer thickness from the experimental ones differs by no more than 5 %, which confirms the accuracy of the obtained models. It was found that during copy-piercing electrical discharge machining in the minimum mode, the continuity of the white layer is on average two times greater than when machining in the maximum mode. The continuity of the white layer of *0.4 C-Cr* steel is 10 % higher compared to *0.35 C-Cr-Mn-Si* steel during copy-piercing electrical discharge machining in the maximum mode and 17 % higher during copy-piercing electrical discharge machining in the minimum mode. It was revealed that when machining in the maximum mode, the number of microcracks is more than 2 times greater than when machining in the minimum mode. The number of cracks in the white layer when processing chromium steels *0.4 C-Cr* and *0.35 C-Cr-Mn-Si* is comparable, the difference does not exceed 10 %.

For citation: Ablyaz T.R., Osinnikov I.V., Shlykov E.S., Kamenskikh A.A., Gorohov A.Yu., Kropanev N.A., Muratov K.R. Prediction of changes in the surface layer during copy-piercing electrical discharge machining. *Obrabotka metallov (tekhnologiya, oborudovanie, instrumenty) = Metal Working and Material Science*, 2025, vol. 27, no. 1, pp. 48–60. DOI: 10.17212/1994-6309-2025-27.1-48-60. (In Russian).

*** Corresponding author**
Shlykov Evgeniy S., Ph.D. (Engineering), Associate Professor
Perm National Research Polytechnic University,
29 Komsomolsky prospect,
614990, Perm, Russian Federation
Tel.: +7 961 759-88-49, **e-mail**: Kruspert@mail.ru

Introduction

The evolution of modern mechanical engineering is intertwined with the development of new, technically advanced products and designs. Manufacturing high-quality products is a primary objective. The operational demands placed on these products are becoming increasingly rigorous, leading to ever-stricter requirements for their performance characteristics. To ensure that products meet the required operational standards, it is essential to utilize materials with enhanced physical and mechanical properties.

Key factors in ensuring a product's competitiveness include its mass and dimensional characteristics. Consequently, increasingly intricate and spatially complex designs are employed, enabling the minimization of product mass and dimensions while still satisfying strength and rigidity requirements.

Traditional machining methods are the most prevalent technologies for manufacturing products with complex geometries. However, conventional blade processing techniques suffer from significant cutting tool wear when processing high-hardness materials. They also require the use of additional equipment for multi-axis machining of complex profiles, and they cannot be used to process thin-walled components due to the force action of the cutting tool [1–3].

When manufacturing complex-shaped products from materials with enhanced physical and mechanical properties, it is advantageous to employ alternative electrophysical processing methods that can process materials of any hardness with virtually no cutting forces. Electrical discharge machining (*EDM*) is one such method [4–10].

A significant disadvantage that limits the application of this electrophysical method is the thermometallurgical transformations that occur in the surface layer of the material being processed. During the removal of material particles from the surface, pyrolysis of the working fluid takes place, leading to changes in the structure and properties of the product's surface layer [11, 12].

The *EDM* process is characterized by localized overheating of the material in the processing zone, which can cause a phenomenon known as *brittle fracture*. In brittle fracture, thermal stresses arise due to overheating of the surface layer of the processed material. When these thermal stresses exceed the material's tensile strength, material is removed from the processing zone. In this case, the material particles are not subjected to melting and evaporation processes but are removed in the solid phase, resulting in chips and cracks [13, 14].

As a result of significant overheating in the processing zone, the material being processed undergoes re-hardening and tempering. Internal stresses arise, which, in conjunction with the altered physical and mechanical properties of the material, can lead to premature product failure during operation or defects during the manufacturing stage [15].

The phenomenon of brittle fracture of the material during *EDM* results in a surface with a high density of microcracks [16]. The presence of microcracks on the working surfaces of the product can lead to its premature failure due to their propagation into the base material, ultimately leading to the failure of a component or the entire product.

The zone of the surface layer containing the greatest number of defects is the so-called *white layer*. The white layer has a fine-grained structure with high chemical resistance. The thickness of the layer varies from tenths of a millimeter to 1.5 mm.

The white layer formed on the surface being processed during the *EDM* process exhibits increased brittleness. Its presence significantly reduces the material's strength characteristics, particularly its resistance to cyclic loads. A review of the literature in the field of *EDM* indicates that an increase in the thickness of the white layer leads to a decrease in the material's fatigue life [17].

The thickness of the white layer and its multiple occurrences on the workpiece surface are determined by numerous factors [18]. One key factor is the processing mode. The electrical process parameters can significantly influence the thickness of the white layer [19]. Increasing current and pulse duration causes a larger volume of material to melt and evaporate due to the increased energy supplied to the workpiece [11]. Reducing the pulse-on time on an electrical discharge machine allows for a decrease in the thickness and continuity of the white layer due to the lower energy input in the processing zone. Decreasing the voltage also leads to a reduction in the white layer thickness [20].

Currently, the formation process of the surface modified layer, as well as the extent of its continuity, and the mechanisms of microcracks formation on the surface of workpieces made of difficult-to-machine materials during copy-piercing electrical discharge machining (*CPEDM*) are not fully studied. The range of materials for which the white layer formation process during machining has been studied is very limited.

An urgent task is to develop theoretical dependencies that allow predicting the transformation of the surface layer during processing, as well as the thickness, structure, and properties of the resulting modified layer.

The aim of this work is a theoretical and experimental investigation of the defective surface layer formed during copy-piercing electrical discharge machining.

Tasks:

1) to develop a theoretical model of a single pulse in the *CPEDM*, applicable to various materials, to predict the white layer thickness; to obtain theoretical values for the white layer thickness for chromium-containing steels *0.4 C-Cr* and *0.35C-Cr-Mn-Si*.

2) to conduct experimental studies of the white layer thickness formed during *CPEDM* to verify the developed models, using chromium-containing steels *0.4 C-Cr* and *0.35C-Cr-Mn-Si* as examples.

3) to conduct experimental studies of the continuity of the white layer after *CPEDM* of chromium-containing steels *0.4 C-Cr* and *0.35C-Cr-Mn-Si*.

4) to conduct experimental studies of the influence of *CPEDM* modes on the number of visible defects on the processed surface of chromium-containing steels *0.4 C-Cr* and *0.35C-Cr-Mn-Si*.

Research methodology

The experiments were conducted at the a Center for Collective Use "*Additive Technologies Center*" within the Department of Innovative Mechanical Engineering Technologies of the Perm National Research Polytechnic University. As part of the study, a unit discharge pulse on the processed surface was simulated using the finite element method (*FEM*). The model consists of three parts: 1) determining the temperature field in the part due to the action of a distributed heat flow; 2) modeling the formation of a pit; 3) determining the temperature field in the part during inter-pulse cooling.

All tasks were solved using the finite element method (*FEM*) with an 8-node element in the *ANSYS Mechanical APDL* package.

The following assumptions and hypotheses were adopted for the solution: isotropy of the workpiece material being processed; temperature-independence of the workpiece material properties; constant convective heat transfer coefficient; negligible energy losses due to changes in the aggregate state of the material; and a constant inter-electrode gap.

The effect of a distributed heat flow on the workpiece-electrode surface is considered.

When modeling a thermal pulse, the effect of a distributed heat flow on the workpiece-electrode surface is also considered.

The heat conduction equation in an axisymmetric formulation for a transient (non-stationary) problem has the form:

$$c \cdot \rho \cdot \frac{\partial T}{\partial t} = -k \cdot \left(\frac{1}{r} \cdot \frac{\partial}{\partial r} \left(r \cdot \frac{\partial T}{\partial r} \right) + \frac{\partial^2 T}{\partial z^2} \right) \quad (1)$$

where r is the current radius; z is the current height.

The ***ABCD*** region represents the area of action of the working pulse (Fig. 1).

On the boundary ***AB***, the condition of axial symmetry for the heat problem applies.

The boundaries ***DE*** and ***EF*** are cooled by the working fluid (*WF*). As a first approximation, these boundaries are modeled as convective heat exchange surfaces, and the convective heat exchange coefficient is assumed to be constant. The condition on these boundaries takes the form:

$$-k \left. \frac{\partial T}{\partial n} \right|_{DE,EF} = h(T - T_\infty) . \quad (2)$$

The thermal insulation condition at the boundaries ***BC*** and ***CF*** has the form:

$$T|_{CD,CF} = 20\ ^\circ\text{C}. \tag{3}$$

The condition on the ***AD*** boundary, assuming a normal distribution, is:

$$-k\left.\frac{\partial T}{\partial n}\right|_{DE,EF} = \eta \cdot \frac{I \cdot U}{\pi \cdot R_p^2} \cdot \frac{1}{\sigma \cdot \sqrt{2\pi}} \cdot e^{\frac{-(r)^2}{2\sigma^2}} \tag{4}$$

The initial condition at all points of the body is taken in the following form:

$$T(0, r, z) = 20\ ^\circ\text{C}. \tag{5}$$

When modeling the inter-pulse cooling process, the scheme shown in Fig. 2 and the equilibrium equation of the heat conduction problem (1) were used.

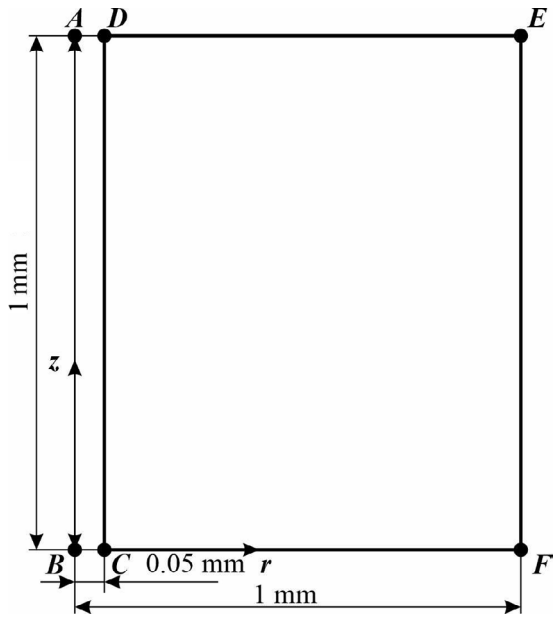

Fig. 1. Design diagram, boundary designation for the working impulse

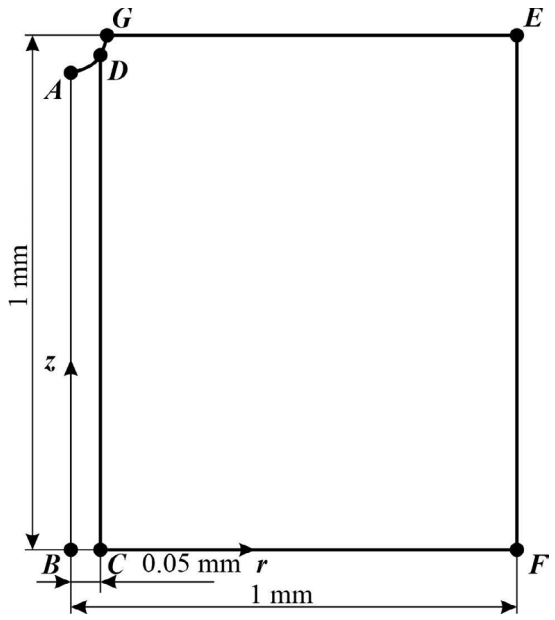

Fig. 2. Design diagram, boundary designation for processes after thermal exposure

On the boundary ***AB*** at ***r*** = 0, the condition of axial symmetry for the heat problem applies.

The boundaries ***AD***, ***DG***, ***GE***, and ***EF*** of the workpiece are cooled by the working fluid (*WF*). As a first approximation, these boundaries are modeled as convective heat exchange surfaces, and the convective heat exchange coefficient is assumed to be constant. The condition on these boundaries takes the form:

$$-k\left.\frac{\partial T}{\partial n}\right|_{AD,DG,GE,EF} = h(T - T_\infty). \tag{6}$$

The thermal insulation condition at the boundaries ***BC*** and ***CF*** has the form:

$$T|_{BC,CF} = 20\,^\circ\text{C}. \tag{7}$$

The initial condition at all points of the body is taken in the following form:

$$T(0, r, z) = T(T_{pulse}, r, z), \tag{8}$$

– temperature field after thermal exposure.

The cooling time was determined taking into account the pulse duty cycle, which was adopted as 26 %.

The simulation was carried out for two *EDM* modes, presented in Table 1.

Within the scope of this study, models were developed for low-alloy *0.4C-Cr* steel and medium-alloy *0.35C-Cr-Mn-Si* steel. The material properties used as input parameters for the modeling are presented in Table 2.

Table 1

Parameters of the copy-piercing *EDM* modes

Parameter	Processing mode	
	min	max
Current ***I***, A	2	8
Voltage ***U***, V	50	100
Pulse duration T_{on}, μs	40	150

Table 2

Input parameters for simulation

Parameter	Designation	Units of measurement	Meaning	
			40C-Cr	*0.35C-Cr-Mn-Si*
Thermal diffusivity coefficient	***K***	W/(m·°C)	46	36
Specific heat	***C***	J/(kg·°C)	466	496
Density	**ρ**	kg/m^3	7,800	7,800
Share of pulse energy	**μ**		0.6	0.6
Heat transfer coefficient	***k***	W/(m·°C)	300	300
Melting point	T_{melt}	°C	1,250	1,280

The solution was implemented using the finite element method. To simulate pit formation, an element was removed when its temperature exceeded the melting point. Element removal was achieved by zeroing the "rigidity" of the elements in the heat problem.

Experiments on the *EDM* of samples were conducted using the same modes as in the simulation (Table 1). An *Electronica Smart CNC* copy-piercing *EDM* machine was selected for the *EDM* of samples made of chromium-containing steels *0.4C-Cr* and *0.35C-Cr-Mn-Si*. Processing was performed in transformer oil environment (*GOST 982-80*).

For experimental studies of the thickness, continuity, and cracking of the white layer formed during *CPEDM*, depending on the processing parameters and the workpiece material, cylindrical samples with a diameter of 35 mm and a length of 20 mm were made from low-alloy *0.4C-Cr* steel and medium-alloy *0.35C-Cr-Mn-Si* steel.

For experiments using the milling method, copper tool-electrodes (*M1* copper grade, *GOST 1173-2006*) with dimensions of 20×20×5 mm were fabricated.

After *CPEDM*, metallographic specimens were prepared. A *Top Tech Presidon* hot mounting press was used to embed the samples in bakelite. Final specimen preparation was performed on a *Top Tech Plato* grinding and polishing unit. Grinding was performed using abrasives with grit sizes ranging from *P240* to *P1500*.

The processed surface was examined for cracks, and metallographic specimens were examined to determine the thickness and continuity of the white layer, using metallographic techniques. Metallographic

examinations were performed using an *OLYMPUS GX 51* optical microscope at ×100-200 magnifications. The *OLYMPUS Stream Motion* software was used for image processing and analysis. To reveal the white layer, the sample metallographic specimens were etched with a 4 % nitric acid solution.

Results and Discussion

The resulting pit formation is shown in Fig. 3.

Fig. 3 illustrates the temperature fields after inter-pulse cooling. The finite element mesh cell size is 5 μm.

During pit formation on the processed surface, a zone remains where the workpiece-electrode material is heated above its melting temperature, followed by instant cooling. This zone is the so-called *white layer*, which concentrates most of the defects. Defects arise due to stresses resulting from re-hardening, and changes in elemental composition caused by saturation of the working fluid and the tool-electrode material with elements.

The developed scheme allows simulating a series of single pulses on the workpiece-electrode surface, taking into account the evolution of the surface geometry. In the future, the developed model can be used to predict the pit size and the overall roughness of the surface processed by *CPEDM*, depending on the processing modes and the properties of the workpiece material.

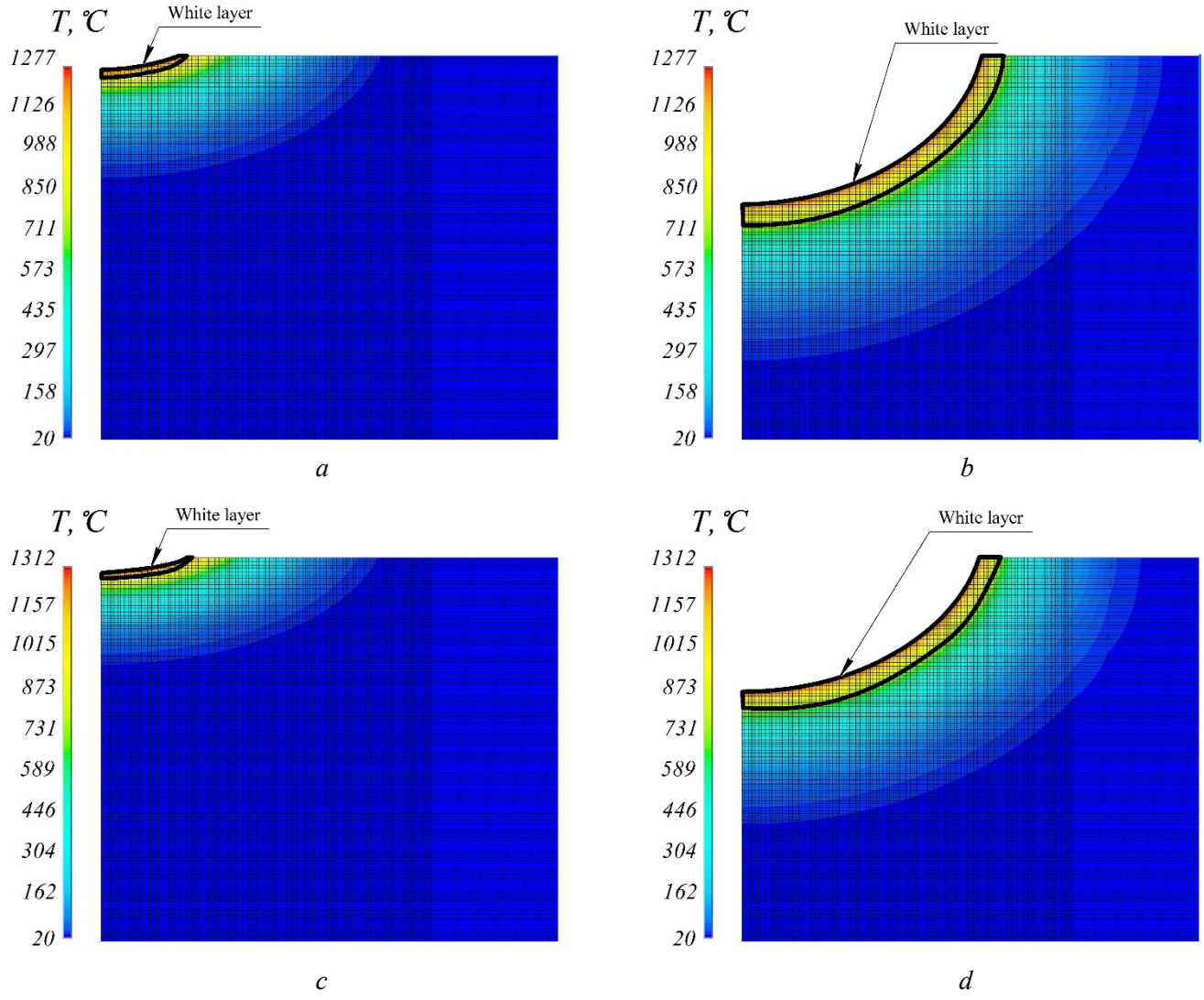

Fig. 3. Temperature distribution fields during crater formation:
a – 0.4 C-Cr, min; *b – 0.4 C-Cr*, max; *c – 0.35 C-Cr-Mn-Si*, min; *d – 0.35 C-Cr-Mn-Si*, max

Table 3 presents theoretical values of the thickness of the white layer formed during *CPEDM*, obtained on the basis the analysis of Fig. 3.

Table 3 presents theoretical values of the thickness of the white layer formed in the CPEDM process, obtained on the basis of the analysis of Fig. 3.

Fig. 4 shows images obtained from metallographic examination of microsections of *0.35 C-Cr-Mn-Si* and *0.4 C-Cr* steel samples after copy-piercing *EDM* at maximum and minimum modes.

Table 3

Theoretical values of white layer thickness

CPEDM mode	Average value of white layer thickness, μm	
	0.4 C-Cr	0.35 C-Cr-Mn-Si
min	25	20
max	80	60

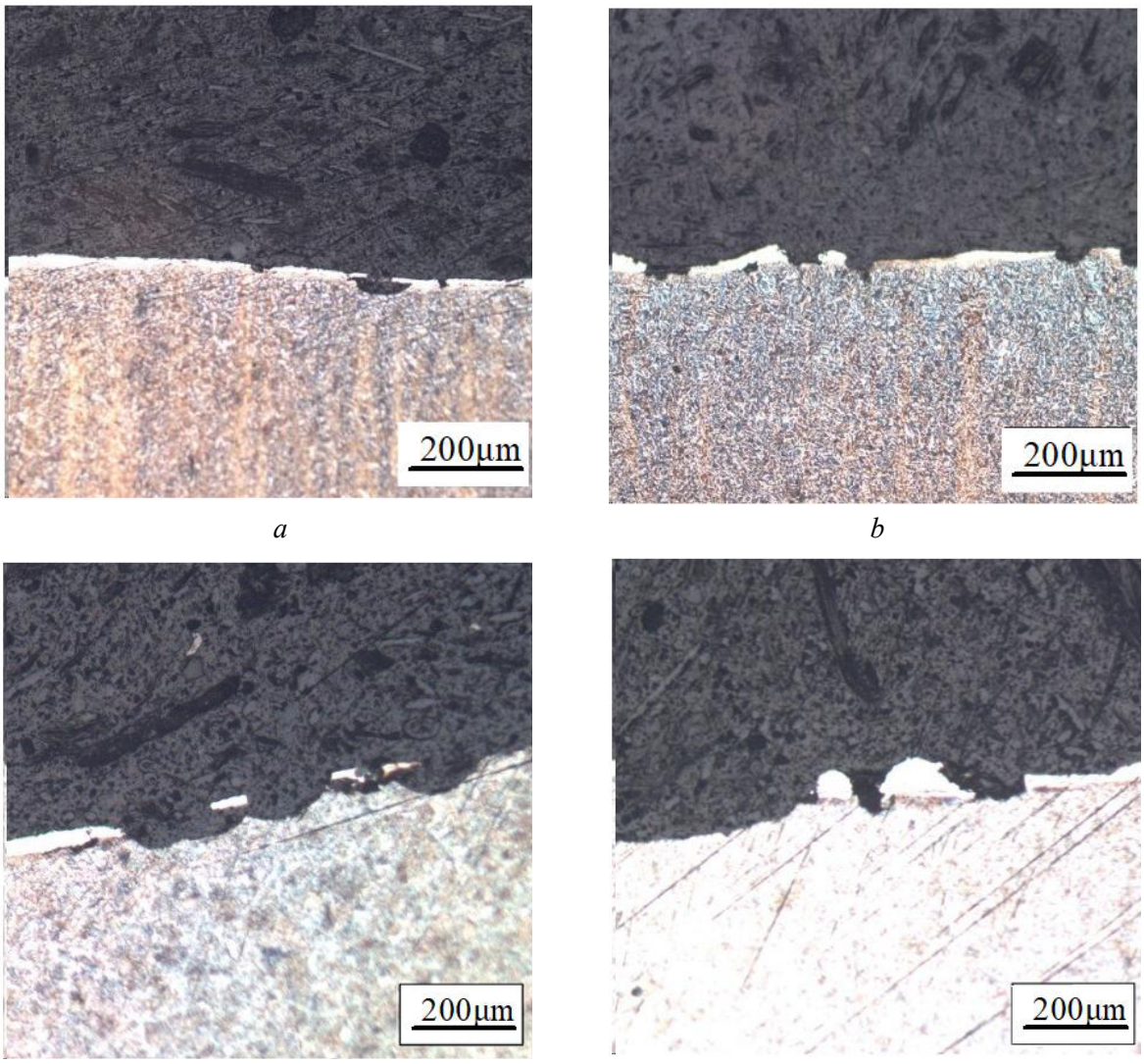

a *b* *c* *d*

Fig. 4. Microstructure of the surface layer of samples after copy-piercing *EDM* at 200× magnification:

a – 0.4 C-Cr, min; *b – 0.4 C-Cr*, max; *c – 0.35 C-Cr-Mn-Si*, min; *d – 0.35 C-Cr-Mn-Si*, max

Visual assessment of the micrographs indicates that a characteristic white layer forms on the processed surface of *0.4 C-Cr* and *0.35 C-Cr-Mn-Si* steels during *CPEDM*. The thickness of this layer varies significantly depending on the processing modes (Table 4).

To compare theoretical and experimental values of the white layer thickness, a histogram was constructed (Fig. 5).

Table 4

Experimental values of white layer thickness

CPEDM mode	Average value of white layer thickness, μm	
	0.4 C-Cr	0.35 C-Cr-Mn-Si
min	23.86	20.79
max	83.00	58.00

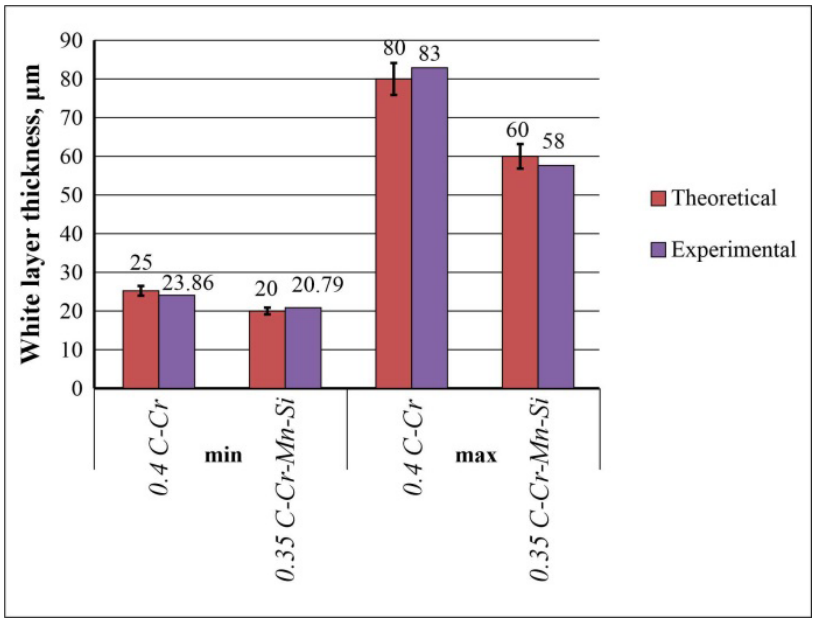

Fig. 5. Histogram of white layer thickness values

Based on the analysis of Fig. 5, the experimental values of the white layer thickness range from 20 to 25 μm for *CPEDM* with the minimum mode and from 55 to 85 μm with the maximum mode.

It has been established that with *CPEDM* under identical conditions, the white layer thickness of low-alloy *0.4 C-Cr* steel is greater than that of medium-alloy *0.35 C-Cr-Mn-Si* steel. This can be attributed to the higher thermal conductivity and lower melting point of *0.4 C-Cr* steel.

A correlation between theoretical and experimental values is observed. The deviation of the theoretical values of the white layer thickness from the experimental values is no more than 5 %, confirming the validity of the obtained models.

The results demonstrate that the developed theoretical models of pit formation during *CPEDM* allow, with the stated accuracy, prediction of the white layer thickness depending on the processing parameters and physical and mechanical properties of the workpiece material.

Based on the analysis of Fig. 4, the white layer formed during CPEDM of *0.4 C-Cr* and *0.35 C-Cr-Mn-Si* steels is distributed unevenly, with numerous voids and cavities observed. To assess the continuity of the white layer, a quantitative assessment of the total area of the white layer on microsections and voids was performed (Table 5).

Based on the obtained data, a histogram was constructed (Fig. 6).

Table 5

Continuity of the white layer of the machined surface after copy-piercing *EDM*

CPEDM mode	Continuity of white layer, %	
	0.4 C-Cr	0.35 C-Cr-Mn-Si
min	94.00	51.00
max	84.00	34.00

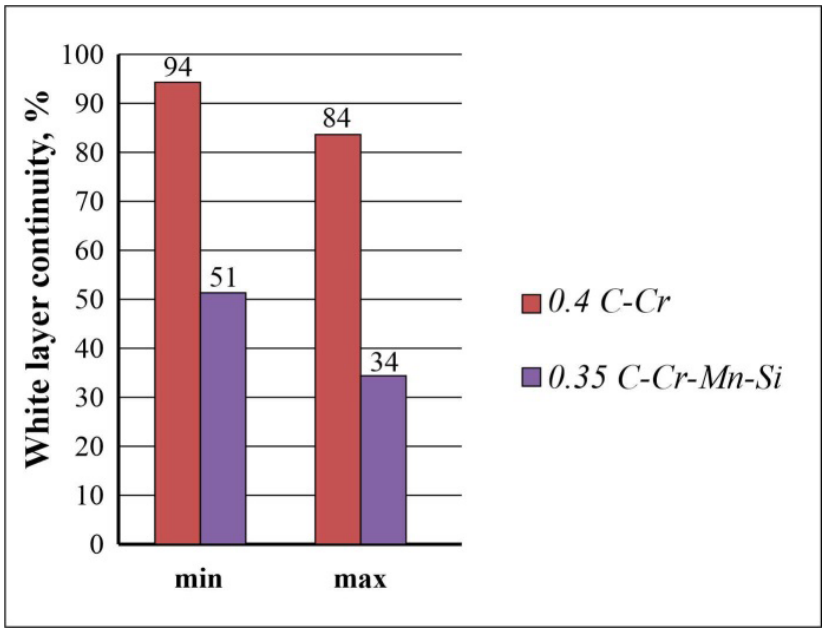

Fig. 6. Histogram of white layer continuity

The histogram analysis showed that the processing parameters significantly affect the continuity of the white layer of processed chromium-containing steels *0.4 C-Cr* and *0.35 C-Cr-Mn-Si*. With *CPEDM* at the maximum mode, the continuity of the white layer is, on average, two times less than when processed at the minimum mode.

It was found that the continuity of the white layer of *0.4 C-Cr* steel is higher than that of *0.35 C-Cr-Mn-Si* steel by 10 % with *CPEDM* at the maximum mode and by 17 % with *CPEDM* at the minimum mode.

Photographs of the processed surface of *0.35 C-Cr-Mn-Si* and *0.4 C-Cr* steel samples are shown in Fig. 7.

Visual assessment of the metallographic examination results showed that numerous microcracks form on the treated surface during the EDM process of *0.35 C-Cr-Mn-Si* and *0.4 C-Cr* steels. An assessment was made of the number of microcracks per unit area of the surface processed by electrical discharge machining. Table 6 presents the results of the quantitative assessment.

Based on the obtained data on the number of microcracks, a histogram was constructed (Fig. 8).

The histogram analysis showed that during *CPEDM* of chromium-containing steels *0.4 C-Cr* and *0.35 C-Cr-Mn-Si*, the number of microcracks formed varies significantly depending on the parameters of the processing mode. The number of microcracks formed during processing at the maximum parameter settings is more than two times greater than that during processing at the minimum parameter settings.

It was established that the number of cracks in the white layer is comparable for *0.4 C-Cr* and *0.35 C-Cr-Mn-Si* steels, with the difference not exceeding 10 %.

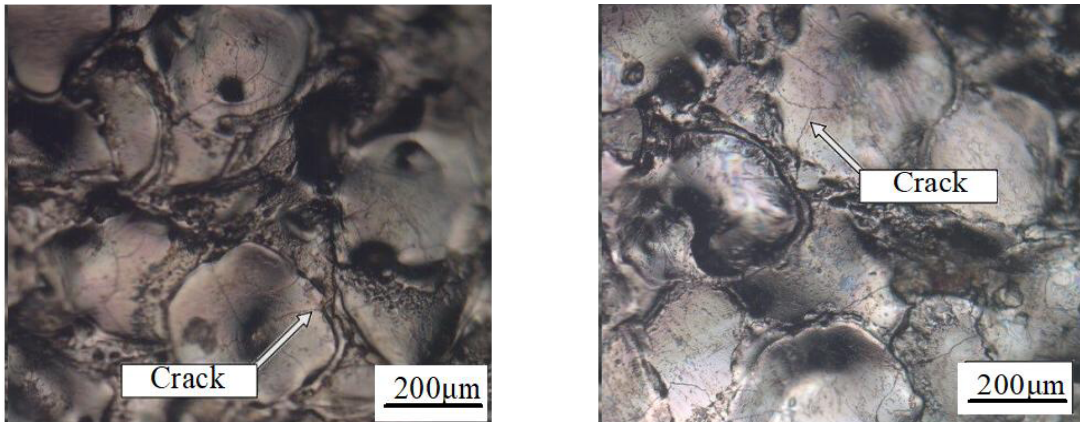

a *b*

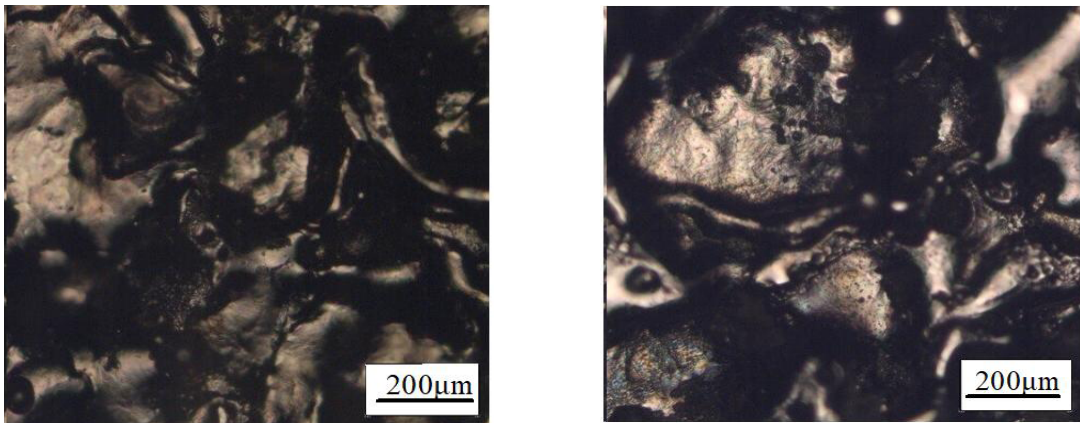

c *d*

Fig. 7. Surface of samples after copy-piercing *EDM* at 200× magnification:
a – 0.4 C-Cr, min; *b – 0.4 C-Cr*, max; *c – 0.35 C-Cr-Mn-Si*, min; *d – 0.35 C-Cr-Mn-Si*, max

Table 6

Number of microcracks on the machined surface after copy-piercing *EDM*

CPEDM mode	Average number of microcracks per 1 mm^2	
	0.4 C-Cr	0.35 C-Cr-Mn-Si
min	28.89	26.38
max	72.35	66.35

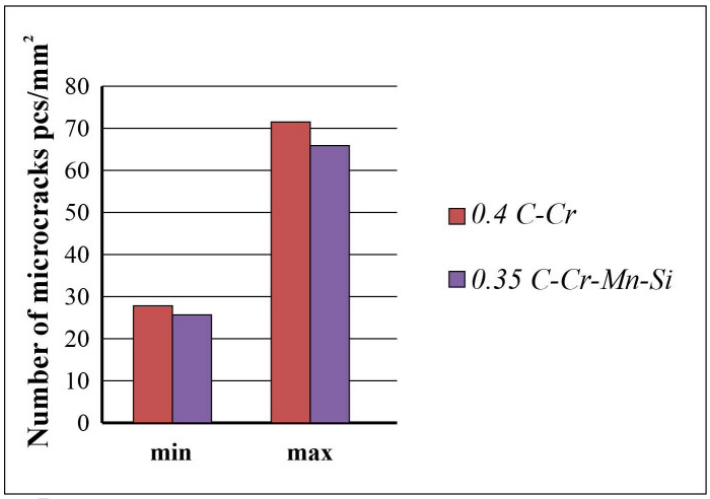

Fig. 8. Histogram of the number of microcracks in the white layer

Conclusions

1. Mathematical models have been developed to simulate the impact of a unit pulse on the processed surface during *CPEDM*, enabling prediction of the white layer thickness based on the processing modes and properties of the workpiece material. The potential for using the developed model to predict the pit size and overall surface roughness has been noted. Theoretical values of the white layer thickness have been obtained for low-alloy *0.4 C-Cr* steel and medium-alloy *0.35 C-Cr-Mn-Si* steel. These theoretical values range from 20 to 25 μm for *CPEDM* at the minimum mode and from 60 to 80 μm at the maximum mode. For *CPEDM* using the same mode, the white layer thickness is greater for low-alloy *0.4 C-Cr* steel than for medium-alloy *0.35 C-Cr-Mn-Si* steel, which can be attributed to the higher thermal conductivity and lower melting point of *0.4 C-Cr* steel.

2. Experimental values of the white layer thickness range from 20 to 25 μm with *CPEDM* at the minimum mode and from 55 to 85 μm at the maximum mode. The developed theoretical models for single-pit formation enable prediction of the white layer thickness with reasonable accuracy, based on processing parameters and the physical and mechanical properties of the workpiece material. The deviation between theoretical and experimental values of the white layer thickness is no more than 5%, confirming the validity of the models.

3. The continuity of the white layer is, on average, twice as great at the minimum mode as at the maximum mode. The continuity of the white layer is greater for *0.4 C-Cr* steel than for *0.35 C-Cr-Mn-Si* steel, by 10 % with *CPEDM* at the maximum mode and by 17 % with *CPEDM* at the minimum mode.

4. The number of microcracks formed during processing at the maximum mode is more than two times greater than that formed during processing at the minimum mode. The number of cracks in the white layer is comparable for *0.4 C-Cr* and *0.35 C-Cr-Mn-Si* steels, with the difference not exceeding 10 %.

References

1. Hawryluk M., Lachowicz M., Zwierzchowski M., Janik M., Gronostajski Z., Filipiak J. Influence of the grade of hot work tool steels and its microstructural features on the durability of punches used in the closed die precision forging of valve forgings made of nickel-chrome steel. *Wear*, 2023, vol. 528–529. DOI: 10.1016/j.wear.2023.204963.

2. Zeisig J., Schädlich N., Giebeler L., Sander J., Eckert J., Kühn U., Hufenbach J. Microstructure and abrasive wear behavior of a novel FeCrMoVC laser cladding alloy for high-performance tool steels. *Wear*, 2017, vol. 382–383, pp. 107–112. DOI: 10.1016/j.wear.2017.04.021.

3. Rogal L., Dutkiewicz J., Szklarz Z., Krawiec H., Kot M., Zimowski S. Mechanical properties and corrosion resistance of steel X210CrW12 after semi-solid processing and heat treatment. *Materials Characterization*, 2014, vol. 8823, pp. 100–110. DOI: 10.3329/jname.v7i2.5309.

4. Dou C., Pan K., Wang C., Wei S., Zhang C., Xu L., Cui H., Liang Y., Huang J. A comparative study on the erosion behavior and mechanism of chrome-coated 25Cr3Mo2WNiV steel and QPQ 25Cr3Mo2WNiV steel. *Materials Today Communications*, 2024, vol. 41. DOI: 10.1016/j.mtcomm.2024.110820.

5. Abbas M.N., Solomon D.G., Bahari Md. A review on current research trends in electrical discharge machining (EDM). *International Journal of Machine Tools and Manufacture*, 2007, vol. 47 (7), pp. 1214–1228. DOI: 10.1016/j.ijmachtools.2006.08.026.

6. Liao Y.S., Chen S.T., Lin C.S. Development of a high precision tabletop versatile CNC wire-EDM for making intricate micro parts // Journal of Micromechanics and Microengineering. – 2005. – Vol. 15. – P. 245–253. – DOI: 10.1088/0960-1317/15/2/001.

7. Yoo H.K., Kwon W.T., Kang S. Development of a new electrode for micro-electrical discharge machining (EDM) using Ti(C, N)-based cermet. *International Journal of Precision Engineering and Manufacturing*, 2014, vol. 15 (4), pp. 609–616. DOI: 10.1007/s12541-014-0378-x.

8. Hoang K.T., Yang S.H. A study on the effect of different vibration-assisted methods in micro-WEDM. *Journal of Materials Processing Technology*, 2013, vol. 213 (9), pp. 1616–1622. DOI: 10.1016/j.jmatprotec.2013.03.025.

9. Hoang K.T., Yang S.H. A new approach for micro-WEDM control based on real-time estimation of material removal rate. *International Journal of Precision Engineering and Manufacturing*, 2015, vol. 16 (2), pp. 241–246. DOI: 10.1007/s12541-015-0032-2.

10. Debroy A., Chakraborty S. Non-conventional optimization techniques in optimizing non-traditional machining processes: a review. *Management Science Letters*, 2013, vol. 4 (1), pp. 23–38. DOI: 10.5267/j.msl.2012.10.038.

11. Świercz R., Oniszczuk-Świercz D., Chmielewski T. Multi-response optimization of electrical discharge machining using the desirability function. *Micromachines*, 2019, vol. 10 (72). DOI: 10.3390/mi10010072.

12. Świercz R., Oniszczuk-Świercz D. The effects of reduced graphene oxide flakes in the dielectric on electrical discharge machining. *Nanomaterials*, 2019, vol. 9 (3). DOI: 10.3390/nano9030335.

13. Chalisgaonkar R., Kumar J. Microstructural characteristics of pure titanium by WEDM. *International Journal of Microstructure and Materials Properties*, 2014, vol. 9 (6), pp. 463–484. DOI: 10.1504/IJMMP.2014.067308.

14. Mouralova K., Zahradnicek R., Benes L., Prokes T., Hrdy R., Fries J. Study of micro structural material changes after WEDM based on TEM lamella analysis. *Metals*, 2020, vol. 10 (7), p. 949. DOI: 10.3390/met10070949.

15. Mehmood S., Sultan A., Anjum N.A., Anwar W., Butt Z. Determination of residual stress distribution in high strength aluminum alloy after EDM. *Advances in Science and Technology Research Journal*, 2017, vol. 11 (1), pp. 29–35. DOI: 10.12913/22998624/68729.

16. Ablyaz T.R., Zhurin A.V., Shlykov E.S. Simulation of electrical discharge machining of dissimilar materials. *ARPN Journal of Engineering and Applied Sciences*, 2018, vol. 13 (6), pp. 2173–2177.

17. Kuo C.-G., Hsu C.-Y., Chen J.-H., Lee P.-W. Discharge current effect on machining characteristics and mechanical properties of aluminum alloy 6061 workpiece produced by electric discharging machining process. *Advances in Mechanical Engineering*, 2017, vol. 9 (11), pp. 1–8. DOI: 10.1177/1687814017730756.

18. Ghodsiyeh D., Golshan A.J., Shirvanehdeh A. Review on current research trends in wire electrical discharge machining (WEDM). *Indian Journal of Science and Technology*, 2013, vol. 6 (2), pp. 154–166. DOI: 10.17485/ijst/2013/v6i2.18.

19. Muthuramalingam T., Saravanakumar D., Babu L.G., Nguen H.P., Vu N.P. Experimental investigation of white layer thickness on EDM processed silicon steel using ANFIS approach. *Silicon*, 2020, vol. 12, pp. 1905–1911. DOI: 10.1007/s12633-019-00287-2.

20. Wijaya H., Wahyudi S., Soenoko R., Setyarini P.H., Yasid S., Gapsari F. The effect of power supply current on recast layer in S45C steel using wire EDM. *IOP Conference Series Materials Science and Engineering*, 2019, vol. 494 (1). DOI: 10.1088/1757-899X/494/1/012102.

Conflicts of Interest

The authors declare no conflict of interest.